TU Delft

Delft University of Technology

Nonlinear dynamic identification of graphene's elastic modulus via reduced order modeling of atomistic simulations

Sajadi, Banafsheh; Wahls, Sander; Hemert, Simon van; Belardinelli, Pierpaolo; Steeneken, Peter G.; Alijani, Farbod

DOI
10.1016/j.jmps.2018.09.013

Publication date
2019

Document Version
Accepted author manuscript

Published in
Journal of the Mechanics and Physics of Solids

Citation (APA)
Sajadi, B., Wahls, S., Hemert, S. V., Belardinelli, P., Steeneken, P. G., & Alijani, F. (2019). Nonlinear dynamic identification of graphene's elastic modulus via reduced order modeling of atomistic simulations. *Journal of the Mechanics and Physics of Solids*, *122*, 161-176. https://doi.org/10.1016/j.jmps.2018.09.013

Important note
To cite this publication, please use the final published version (if applicable).
Please check the document version above.

Copyright
Other than for strictly personal use, it is not permitted to download, forward or distribute the text or part of it, without the consent of the author(s) and/or copyright holder(s), unless the work is under an open content license such as Creative Commons.

Takedown policy
Please contact us and provide details if you believe this document breaches copyrights.
We will remove access to the work immediately and investigate your claim.

This work is downloaded from Delft University of Technology.
For technical reasons the number of authors shown on this cover page is limited to a maximum of 10.

Nonlinear Dynamic Identification of Graphene's Elastic Modulus via Reduced Order Modeling of Atomistic Simulations

Banafsheh Sajadi[a], Sander Wahls[b], Simon van Hemert, Pierpaolo Belardinelli, Peter G. Steeneken, Farbod Alijani[a]

[a]*Precision and Microsystems Engineering, Delft University of Technology, Delft, The Netherlands.*
[b]*Delft Center for Systems and Control, Delft University of Technology, Delft, The Netherlands.*

Abstract

Despite numerous theoretical investigations on the mechanical properties of graphene, an accurate identification of its material behavior is still unattained. One hypothesis for this uncertainty is that modeling graphene as a static membrane cannot describe the strong coupling between mechanics and thermodynamics of this structure. Therefore, characterization methods built upon static models could not capture these effects. In this paper, we propose a new method for building a reduced order model for the dynamics of thermalized graphene membranes. We apply the proper orthogonal decomposition algorithm on time responses obtained from molecular dynamics simulations. As a result, a set of orthogonal modes is obtained which are then employed to build a reduced order model. The proposed model can describe the motion of the suspended graphene membrane over the whole spatial domain accurately. Moreover, due to its computational efficiency, it is more versatile for exploring the nonlinear dynamics of the system. This model is then employed for studying the nonlinear dynamics of graphene membranes at large amplitudes to extract Young's modulus. The obtained Young's modulus incorporates the effects of nano-scaled thermally induced dynamic ripples and hence, is temperature and size dependent. Our proposed atomistic modal order reduction method provides a framework for studying the dynamics and extracting the mechanical properties of other nano-structures at the molecular level.

Keywords: Graphene, Idenification, Nonlinear Dynamics, Molecular Dynamics, Proper Orthogonal Decomposition, Reduced order modeling, Elasticity.

1. Introduction

The fabrication of graphene as a single atom thick membrane has been a promising step towards down-scaling of Nano Electro-Mechanical Systems (NEMS) with potential applications in pressure sensing [1], mass sensing [2, 3], and electronics [4–6]. The proper modeling and characterization of graphene is a crucial step towards the development and commercialization of these advanced applications. For this reason many experimental, theoretical, and computational studies have been performed to investigate the limit of intrinsic mechanical properties of pristine graphene [7–14]. However, there is still a large variation in the experimentally measured Young's modulus of graphene as compared to its theoretical limit [13]. For instance, Atomic Force Microscopy (AFM) measurements have shown a large variation in the values of the Young's modulus from 0.43-1.2 TPa [13, 14], respectively. On the other hand, theoretical methods have resulted in a range of 650 to 1240 GPa for the Young's modulus of graphene depending on the load direction, temperature, the size of the structure [7, 8, 13].

Among others, *ab initio* calculations, Density Functional Theory (DFT), Molecular Mechanics (MM), and Molecular Dynamics (MD) are the most commonly used algorithms for obtaining the material properties of graphene, and in particular its elastic modulus, numerically [15, 16]. These methods are usually based on static approaches, i.e. following the changes in the energy of the system due to a stepwise static displacement at the boundaries of the membrane. By fitting a static continuum based model to the response of such simulations, the Young's modulus is identified.

One hypothesis for the uncertainty in the obtained elastic modulus by these approaches, particularly for relatively small membranes, is the presence of thermally induced dynamic ripples in the membrane (also known as flexural phonons) due to its Brownian motion at finite temperature [7, 9, 17–21]. The dynamic ripples, being of the order of the thickness of a single-layer graphene, are large enough to influence the mechanical response of the suspended membrane and as such, also the obtained equivalent Young's modulus via static approaches. In fact, graphene at finite temperatures behaves as a dynamically corrugated plate and therefore, if it is statically loaded, first, the stretching reduces the number of transverse phonons and ripples, and thus, causes its entropy to reduce, corresponding to an entropic force. The elasticity of graphene is therefore, like a rubber band, not purely due to the atomic potentials, but also governed by its thermodynamics: it acts as an entropic spring at finite temperatures [22]. Only after these transverse phonons have been quenched by tension, the intrinsic elasticity corresponding to atomic potential of the carbon atoms is obtained [19, 23, 24]. Hence, the equivalent stiffness obtained from static approaches exhibits a nonlinear behavior depending on the applied stretch [7, 8, 23, 24]. It is rather difficult to disentangle the two sources of stiffness (from the deformation of the graphene lattice or suppression of flexural phonons), and still capture their interplay in the available approaches.

Due to the presence of continuously appearing and disappearing dynamic ripples in graphene membranes, a proper model for this material in a continuum framework can be also better achieved via a dynamic approach. Such a model, if available, can set the foundation for proper parameter identification of this material. For instance, for identification of Young's modulus, the dynamic characterization of the 2D nano-material using its Duffing-type nonlinear response can be employed [12]. In fact, the stiffness of a membrane in small deflections is dominated by its pretension. In large deflections, an additional nonlinear geometrical stiffness appears in the elastic potential of the system and hence, in the obtained set of equations of motion [11, 25]. As a result, nonlinear effects emerge in the frequency response of the system as a change in the frequency of the peak amplitude. This geometrical nonlinearity is a function of the Young's modulus of the membrane and therefore, can be used for identification of this property [12].

In this paper, a comprehensive numerical method on modeling the dynamics of graphene while accounting for the temperature dependent nano-scaled dynamic ripples is presented. The proposed method is then used for extracting the elastic modulus of single-layer graphene at high frequencies. To achieve this, first, MD is employed to obtain the time response of all atoms of a graphene membrane when excited with an initial velocity. Next, a Proper Orthogonal Decomposition (POD) algorithm is utilized to obtain the Proper Orthogonal Modes (POMs) of the vibrations of the single-layer graphene membrane. Using a Lagrangian approach, the equations of motion are then discretized with the obtained POMs from MD as the admissible basis functions. As a result, a reduced order model consisting of a set of nonlinear ordinary differential equations is obtained. This atomistic reduced order model can capture the dynamics of the graphene membrane on the whole spatial domain accurately, and yet, with much less degrees of freedom. Finally, by minimizing the error between the nonlinear frequency responses of the reduced-order model and MD, the equivalent elastic properties of graphene are estimated at different temperatures. Due to strong reduction in the number of degrees of freedom by POD, the proposed reduced order model is more versatile for studying on the nonlinear dynamics of such a system as compared to the full atomistic models.

In what follows, the proposed atomistic reduced order modeling method is described in details. In Section 2 the method and its mathematical foundations are described and in Section 3 the method is applied to analyze the nonlinear dynamics of graphene membranes to characterize graphene's material properties. Finally conclusions and future outlook are discussed.

2. Methodology

In this section, we describe our approach to model the nonlinear dynamics and to identify the equivalent elastic modulus of graphene membranes. For this purpose, we use a clamped circular graphene membrane, with a radius of 10-18 nm, as our test-case. The choice of circular drums is because 2D NEMS devices with circular shape yield better structural flexibility as compared

to other geometries and have no corners or sharp edges that can induce high residual stresses in practical applications [26, 27]. Moreover, in experimental setups, these nano-resonators are commonly fabricated by transferring graphene flakes on the top of circular cavities [11, 12]. Using such a method, due to the adhesion between graphene and the substrate, the resonator will have fully clamped boundary conditions which is our motive to choose clamped over hinged boundary condition in our simulations.

The flowchart of the nonlinear material parameter identification from MD simulations is given in Figure 1. The steps of this approach are as follows:
Step 1. MD simulations of the thermalized graphene membrane are performed.
Step 2. POD algorithm is employed to obtained a set of POMs that describe the motion of the atoms with minimum error. The Fast Fourier Transform (FFT) is then employed convert the time response into frequency components, and to obtain the frequency associated with the peak amplitude of each POM.
Step 3. By using the Lagrangian approach and by employing the most dominant POMs as the set of basis functions, we obtain a reduced order model comprising a set of nonlinear equations which describe the motion of the membrane. These equations will be in terms of unknown parameters such as Young's modulus, bending rigidity, or pretension.
Step 4. By fitting the results of these equations of motion in the frequency domain to those of the MD simulations, the Young's modulus can be identified.

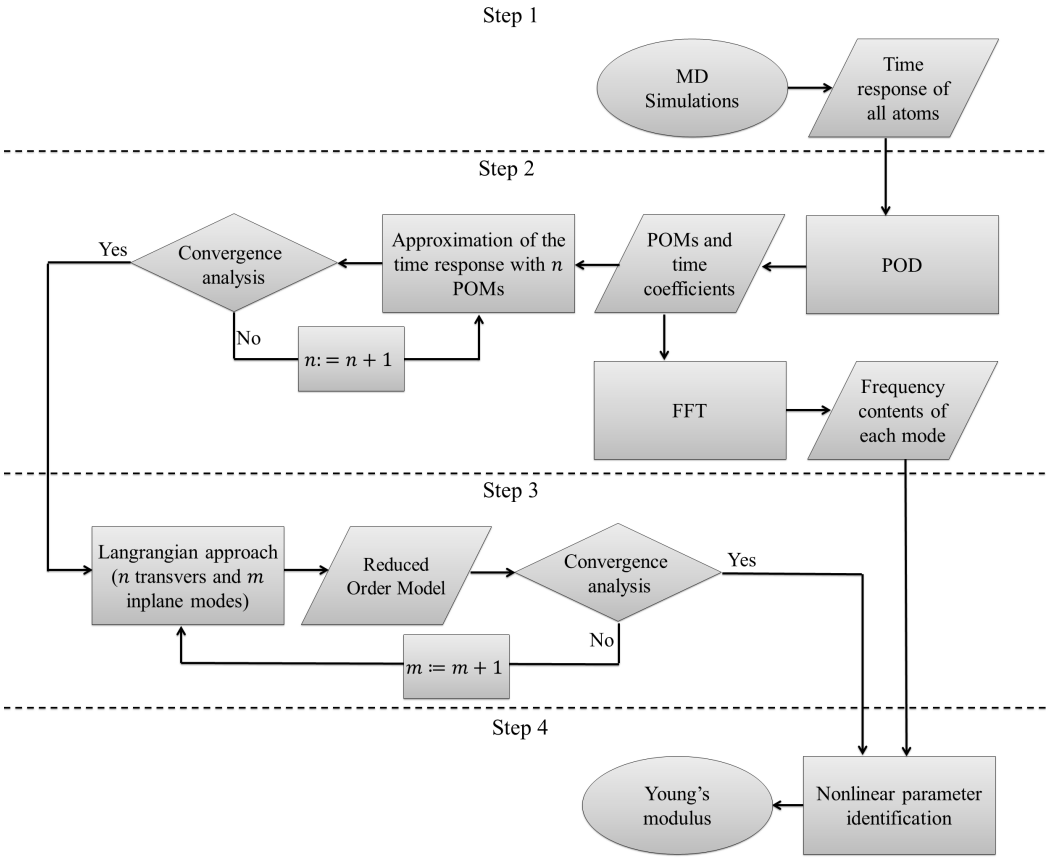


Figure 1: The flowchart of the nonlinear material parameter identification from MD simulations.

In what follows, steps taken will be detailed out.

2.1. Molecular Dynamics Simulations

In the first step, MD simulations are employed to get the time response of all the atoms of an initially excited graphene membrane. For performing the MD simulations, we used the open-source software LAMMPS [28]. In this software, the equations of motion are integrated using the velocity-Verlet integrator algorithm, with a time step of 1 fs. The model consists of a circular flat layer of carbon atoms, ordered in a hexagonal grid with an inter-atomic distance of 1.42 Å. The edges are fully clamped via fixing the position of atoms in three rings of atoms closest to the boundary. The diameter of the drum is 20 nm, and the forces between atoms are described by the Tersoff potential, which is suitable for modeling the atomic interactions in diamond, graphite and graphene [29].

Since the initial position of the atoms may not exactly correspond to equilibrium or the minimum potential state, the system is relaxed by minimization of the total potential energy. The minimization is performed by the Polak-Ribiere conjugate gradient algorithm [30]. The employed objectives in this minimization are 1×10^{-10} eV for energy or 1×10^{-10} eV/Å for force. While relaxing the system, the out of plane coordinates are fixed, to prevent curling of the membrane. Next, the system is allowed to equilibrate in the constant volume and constant temperature ensemble (NVT) using the Nose-Hoover thermostat [31]. This algorithm is performed for 50 ps (i.e. 50000 time steps) to ensure a stable temperature is achieved. During thermalization, the boundaries of the membrane are fixed. This means the membrane will be stretched, as a result of the negative thermal expansion of graphene.

After the temperature is stable, we change the thermostat to an energy conserving ensemble (NVE) [31]. In this step, we excite the membrane with an initial velocity and obtain the amplitude-dependent frequencies of the membrane in a ring-down process. For exciting the membrane around its first resonance, the membrane is actuated by applying a velocity field mimicking the fundamental mode of a membrane in continuum mechanics. To excite the membrane with large amplitudes, different initial velocities are applied, ranging from 0.001 Å/ps to 1 Å/ps. The simulation is performed for a time range of 30 ns. For post processing only a part of the available data, consisting of the time responses of a set of 400 to 1500 atoms out of 13026 atoms, is chosen so as to represent the full structure. The atom coordinates are saved every 0.5 ps (500 time steps), which correspond to approximately 20 points per vibration period of the fifth resonance of the system at 300 K.

2.2. Proper Orthogonal Decomposition

In this section, the decomposition algorithm to obtain a set of basis function from the results of MD simulations is introduced. POD is a tool for extracting spatial and temporal information from a set of numerically generated or experimentally measured time response of a structure at multiple points [32–34]. Although POD has been initially introduced in the field of fluid dynamics for investigating turbulence [35, 36], it has been successfully applied to measure displacement of discrete structures for estimation of normal modes of vibration as well [37–39]. Such a decomposition leads to a set of POMs, by linear summation of which, the snapshots of the measured time response can be expressed with minimum error. These modes can be used as an orthogonal basis for efficient representation of the motion of the structure and hence, can be incorporated for reduced order modeling purposes yielding multiple orders of magnitude reduction in simulation costs [32, 40].

The POD algorithm is as follows. Suppose we have the time history of a vector $\mathbf{u}$ containing the displacement, velocity, or acceleration of a structure at M discrete locations in a domain. The time history consists of N snapshots of the motion as $[\mathbf{u}(t_1), \mathbf{u}(t_2), ..., \mathbf{u}(t_N)]$. We remove the time average (mean values) of the responses, $\mathbf{u}$, by obtaining the time-varying part, $\mathbf{x}(t_i) = \mathbf{u}(t_i) - \text{mean}(\mathbf{u})$. Next, a discrete matrix $\mathbf{X}$ is formed such that each row corresponds to a time response of one location and each column corresponds to a snapshot of the structure at a specific

time:

$$\mathbf{X} = [\mathbf{x}(t_1) \quad \mathbf{x}(t_2) \quad ... \quad \mathbf{x}(t_N)] = \begin{bmatrix} x_1(t_1) & ... & x_1(t_N) \\ . & . & . \\ . & . & . \\ . & . & . \\ x_M(t_1) & ... & x_M(t_N) \end{bmatrix}. \tag{1}$$

where $x_i(t_j)$ is the response at time t_j and location i. The POD of such data can be obtained by using the singular-value decomposition (SVD) of the discrete matrix $\mathbf{X}$. The SVD operator decomposes $\mathbf{X}$ to a factorization of the form:

$$\mathbf{X} = \mathbf{U}\mathbf{\Sigma}\mathbf{V}^*, \tag{2}$$

where $\mathbf{U}$ is an $M \times M$ real or complex unitary matrix, $\mathbf{\Sigma}$ is a $M \times N$ rectangular diagonal matrix with non-negative real diagonals σ_i, $\mathbf{V}$ is an $N \times N$ real or complex unitary matrix, and $\mathbf{V}^*$ is the conjugate transpose of $\mathbf{V}$. The diagonal entries σ_i are known as the singular values of $\mathbf{X}$, and the columns of $\mathbf{U}$ and $\mathbf{V}$ are called the left-singular vectors and right-singular vectors of $\mathbf{X}$, respectively. It can be mathematically shown that the left-singular vectors correspond to POMs that can linearly express all the snapshots of the motion with a minimum error (see Ref. [33]) . We refer to each POM (columns of matrix $\mathbf{U}$) as $\mathbf{\Upsilon_i}$ with $i = 1...M$. The right-singular vectors hold information about the time coefficients of the POMs and the singular values σ_i are the relative kinetic energy captured by each POM.

As a result, each snapshot of the measured time response (x) at the time t_j can be approximated by a linear combination of the obtained modes:

$$\mathbf{x}(t_j) \approx \sum_{i=1}^{M} Q_i(t_j)\mathbf{\Upsilon}_i, \tag{3}$$

where Q_i is the time coefficient (amplitude) of the $i-th$ mode, and can be extracted either directly from $\mathbf{\Sigma}\mathbf{V}$, or equivalently, by using the orthogonality condition of the obtained POMs. According to the orthogonality condition, the inner product of Equation (3) with each POM ($\mathbf{\Upsilon}_i$) gives:

$$\mathbf{\Upsilon}_i.\mathbf{x}(t_j) = Q_i(t_j), \tag{4}$$

where (.) denotes the inner product of two vectors. Since the obtained POMs (the columns of the matrix $\mathbf{U}$) are discrete ($M \times 1$) vectors, to employ them in reduced order modeling, we need to fit a parametrized surface function to each of these modes. Hence, we assume the mode shape to be expressed by an approximate function:

$$\Phi_i(\rho, \theta) = \big(\sum_{k=0}^{K} C_{ki}(\rho)^k\big) \cos\left(B_i\theta + \phi_i\right), \tag{5}$$

where $\rho = r/R$ and θ are polar coordinates, C_k, B_i, and ϕ_i are parameters which are obtained by fitting the function $\Phi_i(\rho, \theta)$ to the vector $\mathbf{\Upsilon_i}$ over the discretized domain. K is the smallest natural number that ensures converged solution. This form of the function is simply chosen due to its resemblance to linear vibration modes of a circular membrane. As a consequence, the measured time response ($\mathbf{x}$) at the time t_j can be approximated by the continuous function:

$$\chi(t_j, \rho, \theta) \approx \sum_{i=1}^{n} Q_i(t_j)\Phi_i(\rho, \theta) \tag{6}$$

where $n < M$ is the minimum number of POMs which shall be adopted to describe the response ($\mathbf{x}$) with the acceptable range of error.

We employ this approach to the time response obtained from MD simulations of initially excited thermalized graphene membrane. For this purpose, the time response of a set of M atoms

chosen to represent the full membrane together with POD algorithm are employed to obtain POMs ($\boldsymbol{\Upsilon}_i$). With Equation (5) these functions can be converted to spatially continuous functions as an orthogonal basis that can be incorporated for reduced order modeling. In addition, the singular values or the relative energy captured by each POM is employed to assess the time evolution of each mode.

2.3. Reduced Order Modeling

In this section, by using the Lagrangian approach and by employing the most dominant modes obtained by POD as the set of basis functions, we obtain a parametrized reduced order model. This model comprises of a set of nonlinear equations which describe the motion of the membrane. For this purpose, the displacements, strains, and strain energies of the membrane are modeled by using the nonlinear von Kármán plate theory, which accounts for finite deflections and moderate rotations [41]. The membrane is assumed to be isotropic and homogeneous [5]. The radius of the membrane is R and its thickness is h. The Young's modulus, bending rigidity, Poisson ratio and the mass density of the membrane are E, D, ν and μ, respectively.

Considering that the initial excitation of the membrane resembles its first radially symmetric first vibrational mode (because this is imposed in the molecular dynamics initial conditions), we assume that the asymmetric in-plane modes which occur at relatively much higher frequencies will not be excited. Hence, for simplicity, we neglect the tangential displacement and only the radial (u) and transverse (w) displacement components are considered. Here, we use a Lagrangian approach to obtain a reduced order set of equations describing the motion of the membrane. In this approach, the displacement components are approximated by the superposition of a finite number of suitably chosen basis functions:

$$w(\rho,\theta,t) = \sum_{i=1}^{n} q_i(t)\Phi_i(\rho,\theta), \tag{7a}$$

$$u(\rho,t) = \xi_0 R\rho + \sum_{i=1}^{m} q_{i+n}(t)R\Psi_i(\rho), \tag{7b}$$

where $\rho = r/R$ and θ are the polar coordinate, and, $q_i(t)$ are dimensionless generalized coordinates. The parameter ξ_0 models the initial uniform strain due to the pretension N_0 in the membrane:

$$\xi_0 = \frac{N_0(1-\nu)}{Eh}. \tag{8}$$

The functions $\Phi_i(\rho)$, and $\Psi_i(\rho)$ are basis-functions satisfying the boundary conditions. Here, the POMs obtained from Equation (5) are utilized as the transverse basis-functions $\Phi_i(\rho)$ to capture the spatial motion at the atomistic level. It should noted that in the current approach, since the transverse mode shapes are adopted from POD algorithm, direct implementation of the boundary conditions will not be required. In other words, our method is capable of capturing the effect of boundary conditions implemented in MD directly in the CM model. For the in-plane basis-functions (Ψ_i), polynomials satisfying continuity and symmetry at $\rho = 0$, are adopted:

$$\Psi_i(\rho) = \rho^i(1-\rho), \qquad i = 1...m. \tag{9}$$

Next, the strain components of the membrane are calculated as [41]:

$$\varepsilon_r = \frac{1}{R}\frac{\partial u}{\partial \rho} + \frac{1}{2R^2}\left(\frac{\partial w}{\partial \rho}\right)^2, \tag{10a}$$

$$\varepsilon_\theta = \frac{1}{R}\frac{u}{\rho} + \frac{1}{2R^2}\left(\frac{\partial w}{\rho \partial \theta}\right)^2, \tag{10b}$$

$$\varepsilon_{r\theta} = \frac{1}{R^2}\frac{\partial w}{\partial \rho}\frac{\partial w}{\rho \partial \theta}, \tag{10c}$$

$$\kappa_r = -\frac{1}{R^2}\frac{\partial^2 w}{\partial \rho^2}, \tag{10d}$$

$$\kappa_\theta = -\frac{1}{R^2}\left(\frac{\partial w}{\rho \partial \rho} + \frac{\partial^2 w}{\rho^2 \partial \theta^2}\right), \tag{10e}$$

$$\kappa_{r\theta} = -\frac{2}{R^2}\left(\frac{\partial^2 w}{\rho \partial \rho \partial \theta} - \frac{\partial w}{\rho^2 \partial \theta}\right), \tag{10f}$$

The total potential energy of the system consists of the potential associated with elastic deformation due to the stretching (U_s) and the bending (U_b) of the membrane [42];

$$U = U_s + U_b, \tag{11}$$

which can be approximated by:

$$U_s = \frac{EhR^2}{2(1-\nu^2)}\int_0^{2\pi}\int_0^1 \left(\varepsilon_r^2 + \varepsilon_\theta^2 + \quad 2\nu\varepsilon_r\varepsilon_\theta + \frac{1-\nu}{2}\varepsilon_{r\theta}^2\right)\rho \mathrm{d}\rho \mathrm{d}\theta, \tag{12}$$

$$U_b = \frac{D}{2}\int_0^{2\pi}\int_0^1 \left(\kappa_r^2 + \kappa_\theta^2 + \quad 2\nu\kappa_r\kappa_\theta + \frac{1-\nu}{2}\kappa_{r\theta}^2\right)\rho \mathrm{d}\rho \mathrm{d}\theta, \tag{13}$$

The kinetic energy of the system can be expressed as:

$$T = \pi\mu R^2 h \int_0^1 (\dot{w}^2 + \dot{u}^2)\rho \mathrm{d}\rho, \tag{14}$$

where overdot indicates differentiation with respect to time. When the membrane is excited around its first resonance, in-plane displacement u is a higher order function of w, and hence, $\dot{u}^2$ can be neglected as compared to $\dot{w}^2$. Employing the relations given in Equations (7a)–(14), the Lagrangian of the system $L = T - U$ can be expressed in terms of generalized coordinates $L(q_i, \dot{q}_i, t)$, and the Lagrange equations can be employed to obtain the equations of motion:

$$\frac{\partial L}{\partial q_i} = \frac{\mathrm{d}}{\mathrm{d}t}\left(\frac{\partial L}{\partial \dot{q}_i}\right). \tag{15}$$

As a result of neglecting the radial inertia, Equation (15) leads to a system of nonlinear equations comprising n differential equations associated with the transverse generalized coordinates and m algebraic equations for in-plane degrees of freedom. The system of differential equations associated with the transverse generalized coordinates can be expressed as:

$$\bar{\bar{\mathbf{M}}}\ddot{\mathbf{q}} + [\bar{\bar{\mathbf{K}}}(N_0, D) + \bar{\bar{\mathbf{N}}}_{\mathbf{3}}(\mathbf{q})]\mathbf{q} = \mathbf{0}, \tag{16}$$

where $\bar{\bar{\mathbf{M}}}$ is the mass matrix, $\bar{\bar{\mathbf{K}}}$ is the linear stiffness matrix and accounts for the pretension and bending stiffness, $\bar{\bar{\mathbf{N}}}_{\mathbf{3}}$ is matrix representing the cubic (Duffing) nonlinearity due to geometrical stiffness, respectively, and is a function of the elasticity of the membrane. The natural frequencies of such a system ω_i are obtained from the characteristic equation of the linearized system (i.e. $\det[\omega_i^2\bar{\bar{\mathbf{M}}} - \bar{\bar{\mathbf{K}}}] = 0$).

In order to obtain adequate number of transverse and in-plane basis functions (n and m), the convergence of the periodic solutions and the frequency response of the system at large amplitudes for a set of assumed material parameters is studied. For this convergence analysis, $\mathbf{q}$ is determined at different amplitudes by considering different number of degrees of freedom. We seek periodic solutions in a regime of free vibrations by building a one-dimensional family of orbits parameterized with respect to the orbit period. These responses subsist only for zero damping and constitute the so-called "backbone curve" [43]. The numerical solutions are obtained with the toolbox "COCO" for continuation along families of periodic orbits [44]. The backbones are obtained by releasing simultaneously both the system period and damping and allowing these to vary during the continuation. Nevertheless, the damping value remains approximately 0 ($\mathcal{O}(10^{-15})$), since unforced periodic orbits with nonzero amplitude exist only if damping is zero.

2.4. Nonlinear Parameter Identification

In this section, based on the results of the convergence analysis, we assume that the large amplitude vibrations of the graphene membrane around its fundamental frequency can be expressed by including a single transverse mode shape only (i.e. in Equation (16), $n = 1$). The validity of this assumption will be discussed in the next section. In this case, the reduced order model obtained by using the POMs will be simplified to a Duffing equation, which if divided to the first modal mass, can be expressed as follows:

$$\ddot{q_1} + \omega_0^2 q_1 + k_3 q_1^3 = 0, \tag{17}$$

where ω_0 is the natural frequency of the system. The parameter k_3 is the cubic spring constant and is a function of the Young's modulus and Poisson's ratio, and its convergence and accuracy is determined by using different number of terms in the expression of the radial displacement (m in Equation 7b). It should be noted that the expressions of k_1 and k_3 depend on the employed basis functions in the Lagrangian approach and for example, these expressions would be different for a classical membrane or plate, as compared to the obtained modes from POD. In this study, k_3 is employed as the fitting parameter to minimize the error between the continuum model and the results of the MD simulations, which leads to identification of the equivalent Young's modulus.

The effect of cubic nonlinearity only gets dominant in large amplitudes of vibrations [12]. As a consequence of this nonlinearity, the frequency of the peak amplitude increases when the amplitude of vibration is increased. In order to obtain the relation between the nonlinear behavior and the cubic nonlinearity, here, we utilize the harmonic balance method [43]. This method entails the solution of nonlinear equations to be approximated by a steady state truncated Fourier series. With such assumption, the frequency of the peak amplitude (q_{max}) approximately occurs at the the backbone curve given by [45]:

$$\omega_{backbone}^2 = \omega_0^2 + \frac{3}{4} k_3 q_{max}^2 \tag{18}$$

By fitting Equation (18) to the amplitude versus frequency curves obtained from MD simulations, the parameter k_3 can be estimated and hence, the Young's modulus can be identified. For this purpose, the frequency and amplitude of vibrations shall be extracted from the time response of the atoms from the MD simulations. The amplitude of vibrations is approximated by Equation (6) and the fundamental frequency (frequency at which the system tends to oscillate without driving force) is obtained by FFT of the time response. The frequency associated with the peak amplitude of the each POM can be obtained by employing FFT on the time history of its coefficient Q_i derived from POD algorithm.

It is worth noting that the proper choice of the time range to extract the amplitude and frequency from MD simulations is a key step in this process. In fact, to get an accurate estimation of the amplitude and natural frequencies of the system, the FFT algorithm shall be performed on the steady-state time response. However, as it will be shown in Section 3, when graphene is excited with an initial velocity, due to the equipartition of energy, the energy applied to the system leaks to higher modes of vibration and therefore, the amplitude and frequency of the first mode will be

continuously decreasing. This decrease has a much higher rate at the begining. If the simulation time is long enough so that the motion of the graphene is steady, the amplitude of vibration will be relatively small and as a result, the effect of cubic nonlinearity on the frequency associated with the peak amplitude will be negligible. Moreover, due to energy transfer from the first mode, the amplitude of this mode becomes small such that Equation (17) will not be valid anymore. To avoid this problem, we employ the time evolution of the energy of the POMs to find a time domain in which (i) the measured response is steady, (ii) the vibrations are still at relatively large amplitudes, and (iii) the time response is periodic and can be approximated by employing POMs. We will show in the proceeding section that the proper choice of the time domain for performing our dynamic analysis can be justified by observing the kinetic energy of the fundamental mode of vibration. In particular, we find that in all our studied cases, a steady state response can be assumed in a time range where the energy transfer between the fundamental mode of vibration and other modes is less than 5% per ns. Moreover, to ensure geometric nonlinear vibrations, we excite the membrane with different initial velocities in such a way that a shift of 10% or higher is observable in the fundamental frequency of the membrane with respect to that obtained from the spectrum of its Brownian motion.

The natural frequency and amplitudes obtained from the measured time response from MD simulations are then utilized to form the backbone curve. By fitting Equation (18) to the data from MD simulations, the parameters ω_0 and k_3 and thus, the equivalent Young's modulus can be estimated.

3. Results and Discussion

In this section, we discuss the results of the proposed identification algorithm in Section 2 for a single-layer graphene membrane. The results are first discussed for a membrane with 20 nm diameter at 300 K and later, the temperature and size dependency of the results will be addressed.

First, in order to investigate the time evolution of the results, the MD simulations are performed over a long time range of 30 ns, and the POD algorithm is performed for time ranges of 0.25 ns in every 5 ns. A snapshot of the motion of the graphene membrane excited with an initial velocity of 0.5 Å/ps, together with its first eight POMs are illustrated in Figures 2, 3, and 4.

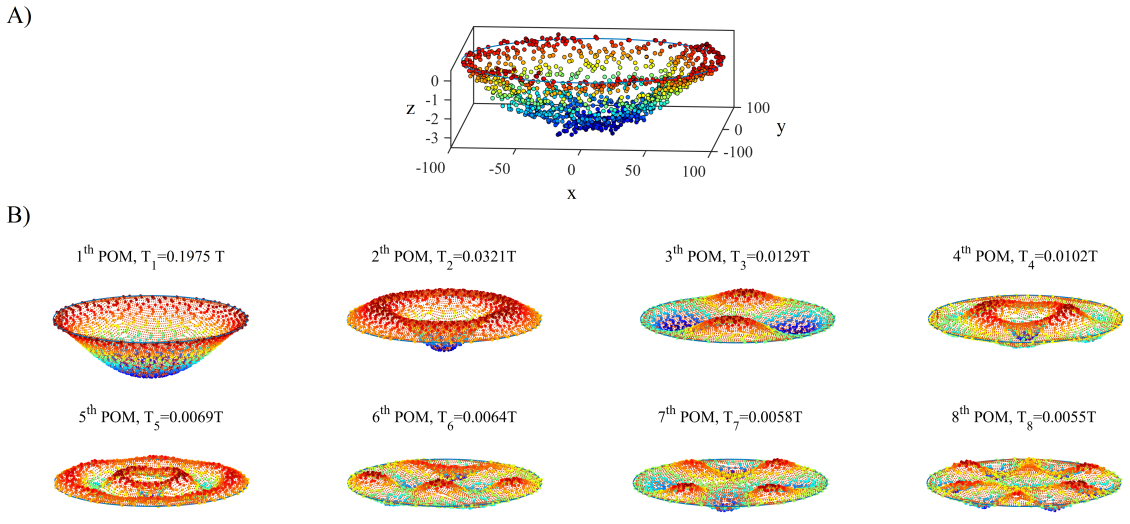


Figure 2: A) The positions of the chosen subset of atoms in Cartesian coordinate in Å, in a snapshot of the motion of the graphene membrane excited with an initial velocity mimicking the first mode shape with a maximum of 0.5 Å/ps in a time range of 5 to 5.25 ns, B) the first 8 POMs, T_i is the relative energy captured by each POM in the specified time domain

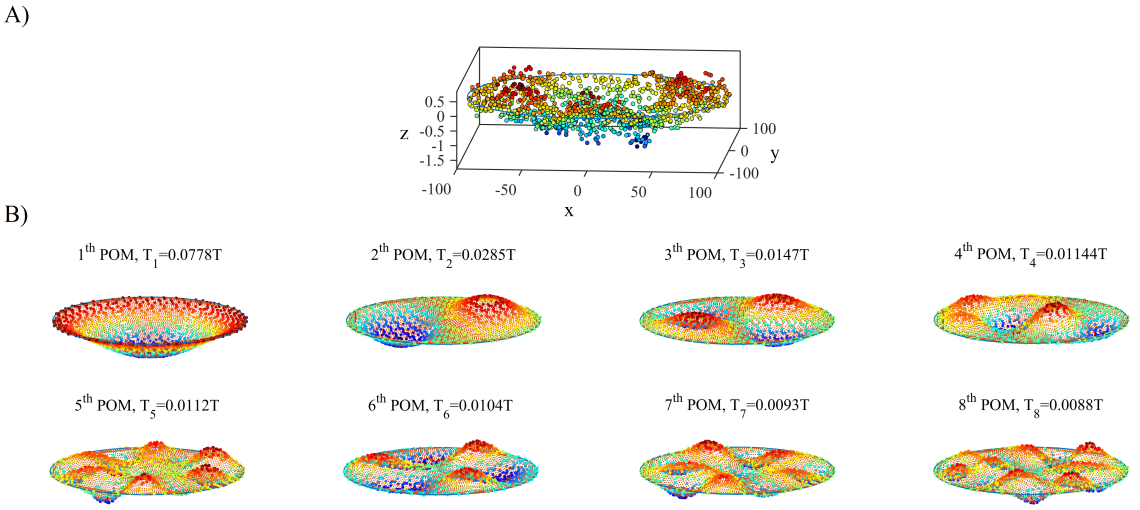


Figure 3: A) The positions of the chosen subset of atoms in Cartesian coordinate in Å, in a snapshot of the motion of the graphene membrane excited with an initial velocity mimicking the first mode shape with a maximum of 0.5 Å/ps in a time range of 20 to 20.25 ns, B) the first 8 POMs, T_i is the relative energy captured by each POM in the specified time domain.

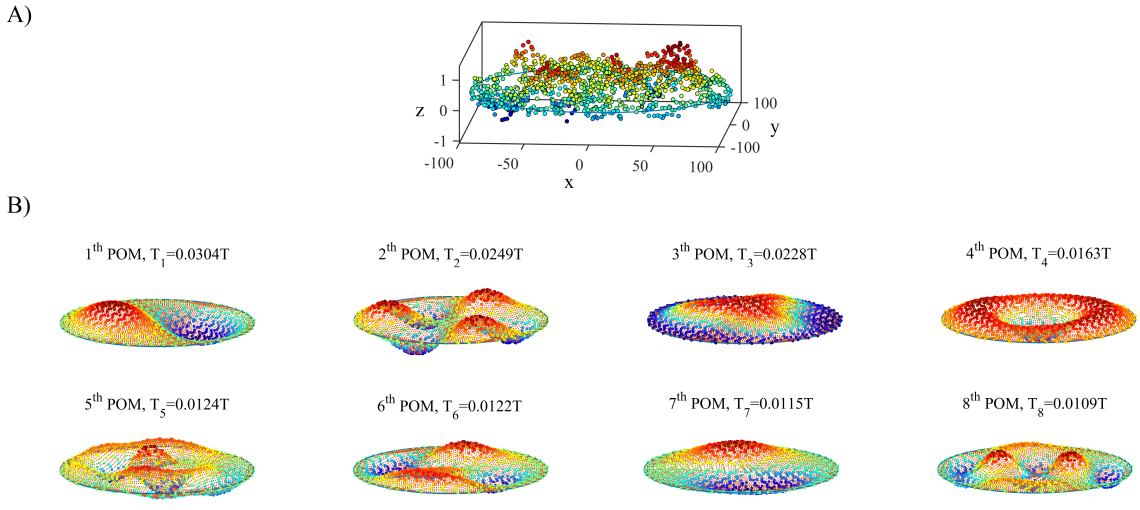


Figure 4: A) The positions of the chosen subset of atoms in Cartesian coordinate in Å, in a snapshot of the motion of the graphene membrane excited with an initial velocity mimicking the first mode shape with a maximum of 0.5 Å/ps in a time range of 30 to 30.25 ns, B) the first 8 POMs, T_i is the relative energy captured by each POM in the specified time domain.

These figures are obtained for time ranges of 5 to 5.25 ns, 20 to 20.25 ns, and 30 to 30.25 ns, respectively. Moreover, the relative energy captured by each POM in the specified time domain which is obtained from singular values of Equation (2) is indicated in these figures. As it can be observed from the snapshots of the motion, although the graphene membrane has been excited with an initial velocity mimicking the first mode, after only a few nanoseconds, the dynamic ripples start to appear in the motion of the membrane and their effects gradually get more and more dominant.

The first eight POMs of the motion in different time ranges in Figures 2, 3, and 4 are ordered with their relative energy. At 5 ns, the first POM (with an approximately similar shape to the

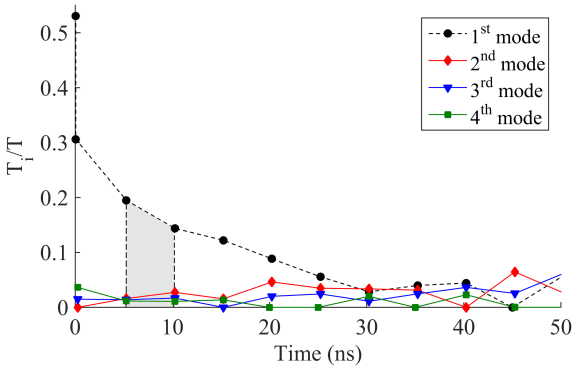


Figure 5: Time evolution of the relative kinetic energy of the first four modes based on their frequency order, for a graphene membrane excited with an initial velocity of 0.5 Å/ps in a time range of 0-50 ns obtained from MD simulations.

imposed velocity), has approximately 20% of total transverse kinetic energy (see Figure 2-B), while this number reduces to 8% at 20 ns (Figure 3-B), and to less than 3% at 30 ns (Figure 4-B). In fact at 5 ns, the motion of the membrane is dominated by its vibrations at its natural frequency, while, at 30 ns, the relative energy of all POMs are in a similar range (<4%). It is interesting to notice that the POM resembling the shape of the fundamental mode of the membrane becomes the 3rd POM at 30 ns. In this situation, the motion of the membrane resembles a random Brownian motion rather than an imposed vibration with a defined shape.

It is worth to note that at first 5 ns, the kinetic energy of the first POM is first transferred to the other axi-symmetric modes (see Figure 2-B). However, after 20 ns, different and rather random modes of vibration appear for a short time and then, disappear due to the transfer of their energy to the other modes. After 30 ns, there is hardly any clear vibration excluding the continuously appearing and disappearing dynamics ripples and, as a matter of fact, the total initial kinetic energy given to the system is transformed into the thermal energy. However, since the added energy is much lower as compared to the total energy, it mildly increases the overall temperature.

Figure 5 illustrates the time evolution of the relative kinetic energy of the POMs of a graphene membrane excited by an initial velocity of 0.5 Å/ps in a time range of 0-50 ns. These modes are numbered with the order of their peak frequency (from FFT). At first 100 ps, the imposed kinetic energy is transferred from the first mode to the other modes of vibration at a very high rate. However, the rate of this energy transfer reduces to a large extent at 5 ns. After 25 ns, the energy transfer has a very low rate and in fact, it occurs more randomly from all modes. At this point, in order to simulate the dynamics of graphene with the proposed reduced order model, we need to include a large number of modes. Moreover, the amplitude of vibrations at this time range are not large enough such that the effect of geometrical stiffness on the frequency associated with peak amplitude to be significant. Hence, the time range of 5-10 ns is chosen for obtaining the mean amplitude and frequency of vibrations so that the motion of the graphene membrane is almost steady-state and the amplitude is large enough such that the frequency response is nonlinear. In this time range the average rate of energy transfer from the first mode to the other modes for all the imposed initial velocities is less than 5% per ns, which justifies the time response of this mode as steady state. Moreover, in this time range, the first mode has the most contribution in the motion.

As mentioned in Section 2.4, the natural frequency of the graphene membrane is obtained by taking the FFT of the time response from MD simulations. The time evolution of the FFT of the out-of-plane motion of a graphene membrane, and over a time range of 5-10 ns, for an initial velocity of 0.5 Å/ps, are shown in Figure 6-A and -B, respectively. As it can be observed in Figure 6-A, the frequency associated with the peak amplitude is reducing over time. At the beginning (0-5 ns), the energy of the first mode is high and its amplitude is large. Therefore, a significant geometrical stiffness is induced in the system which leads to a larger natural frequency.

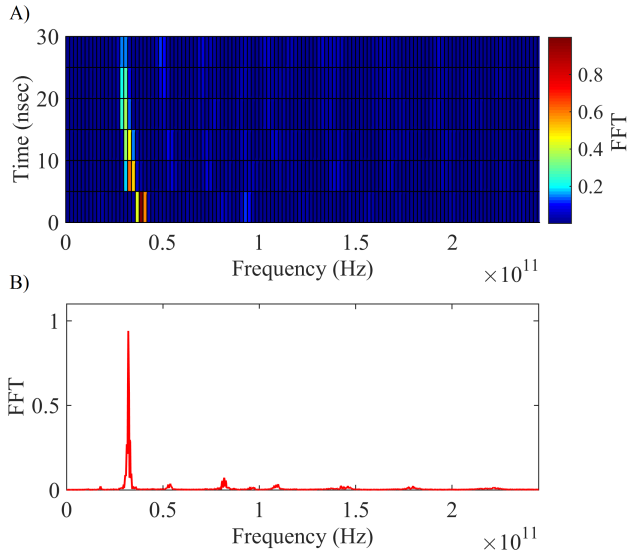


Figure 6: A) The time evolution of the Fast Fourier transform (FFT) for the out-of-plane motion of a graphene membrane obtained from MD, B) FFT of the time response in a time range of 5-10 ns, for an initial velocity of 0.5 Å/ps.

As the energy of the first mode reduces with time, its amplitude decreases and so do the resulted geometrical stiffness and the frequency of the peak amplitude. Figure 6-A shows that at 5 ns and 10 ns, the nonlinear hardening is still apparent in the dynamics of the system and yet, the rate of the changes are much lower as compared to 0 ns. In fact, in this time range, the shift in the natural frequencies at large initial velocities (i.e. 0.5-1 Å/ps) is 10-12%, which confirms the suitability of this time range for performing parameter identification. For other radii or geometries of the membrane, the given initial velocities should be adapted to observe similar range of shift in the frequencies.

It is worth noting that the obtained POMs and their associated peak frequency are temperature dependent. In fact, the thermal vibrations of the atoms of graphene, not only change the tension in the membrane but also affect the shape of the POMs. The transverse deflection of the membrane can be approximated by substituting the obtained POMs and their time coefficient in Equation (3). The number of the POMs adopted for this approximation depends on the time range and the amplitude of vibrations. Figures 7 and 8 illustrate the approximated deflection at the center of the membrane for different initial velocities and time ranges.

Figure 7 shows the time response at the center of the graphene membrane excited with an initial velocity of 0.5 Å/ps, obtained from MD (blue dots) and approximate solution obtained from POD with adopting 1 mode (red line) and 10 modes (black line) in different time ranges. These approximations are obtained by using Equation (3). It can be observed that the amplitude of the motion decreases with time and the higher frequency modes with low amplitude become more dominant in the motion at the center of the membrane. In addition, in the time range of 0–10 ns, the motion is strongly dominated by the first mode. In fact, in this time range, if the motion is approximated with a single mode only, the average error of this approximation is less than 0.33 Å. Moreover, in this time range, the difference between approximating with 1 and 10 modes is negligible. Clearly, the accuracy of the approximation reduces at 30 ns, but still, retaining 10 modes results in a slightly better approximation than 1 mode only.

Figure 8 shows the time response of the center of the graphene membrane excited with different initial velocity of 0.1 Å/ps, 0.5 Å/ps, and 1 Å/ps, in a time range of 5–5.15 ns. The graphs in this figure are obtained by MD (blue dots) and POD with adopting 1 mode (red line) and 10 modes (black line). This figure shows that in all three cases, the motion is highly influenced by the first mode and the difference between employing 1 and 10 modes in approximating the motion

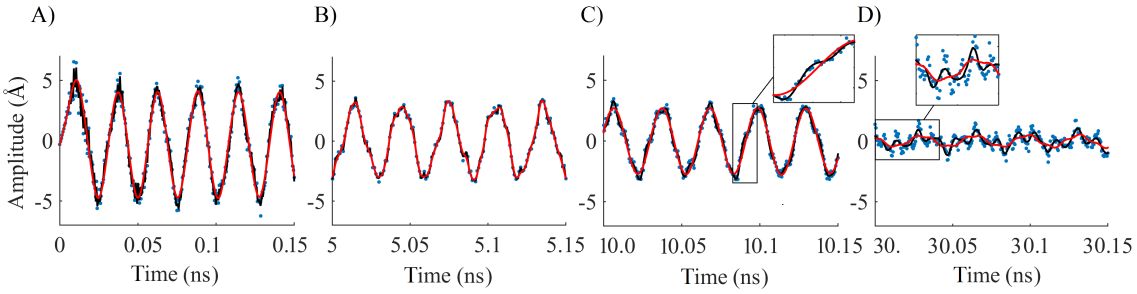


Figure 7: Time response of the center of the graphene membrane excited with an initial velocity of 0.5 Å/ps, obtained from MD (blue dots) and POD with adopting 1 mode (red line) and 10 modes (black line) in time ranges of (A) 0–0.15 ns, (B) 5–5.15 ns, (C) 10–10.15 ns, and (D) 30–30.15 ns.

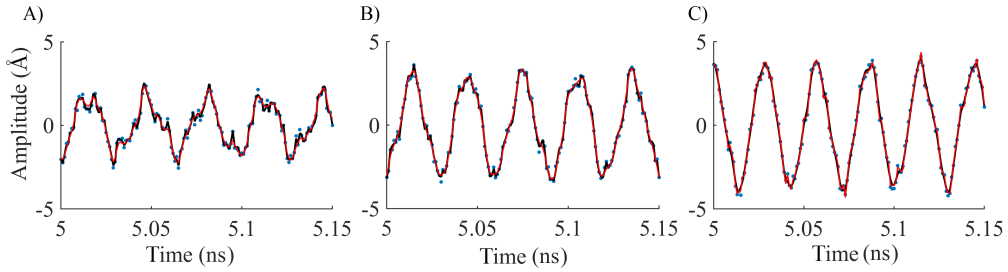


Figure 8: Time response of the center of the graphene membrane excited with different initial velocities of A) 0.1 Å/ps, B) 0.5 Å/ps, and C) 1 Å/ps obtained from MD (blue dots) and approximation obtained from POD with adopting 1 mode (red line) and 10 modes (black line) in a time range of 5–5.15 ns.

is negligible. However, at large amplitude vibrations the effects of dynamic high frequency modes is less dominant and hence, the relative error in approximating the motion with a single mode is smaller than low amplitude vibrations. In the time range of 5-10 ns, the average error of an approximation with 1 mode for all the imposed initial velocities is 0.22 Å, which shows the accuracy of approximating the motion with 1 mode only, and justifies the suitability of the time domain in which our nonlinear identification will be performed. In fact, the dynamic ripples which occur at very high frequencies have much lower amplitudes as compared to the imposed motion due to the initial velocity. Moreover, the motion at larger amplitudes is approximately periodic and hence, the harmonic balance can be employed to simplify the motion at such amplitudes more accurately. For this reason, in the identification process we employ the data from MD simulations for membranes that are excited with initial velocities of more than 0.5 Å/ps.

Next, for nonlinear parameter identification, the POD algorithm is performed for a long time range of 5-10 ns. The time response of the center of the graphene membrane extracted directly from MD (black line) and the coefficient of the first POM (red line), in the time range of 5 to 10 ns, are illustrated in Figure 9. As it can be observed, the motion of the membrane in this time range is highly dominated by the first mode only. Moreover, the amplitude of vibrations is approximately steady in this range.

To form the basis functions for reduced order modeling, the discrete POMs are approximated by continuous functions as expressed in Equation (5) with least squares method. The cross section of the approximated shape functions for the first three mode shapes (ordered by their associated frequency) are shown in Figure 10. For comparison, the vibration modes of an equivalent classical plate, are illustrated in this figure as well. As it can be observed, the mode shapes of the graphene membrane is different from a classical plate. This difference is due to (i) presence of thermally induced ripples and (ii) different bending stiffness of graphene as compared to a plate. In this paper, in order to capture the difference of the graphene membrane with an ideal membrane, not only we use the actual modes obtained from POD algorithm, but also, we employ the finite

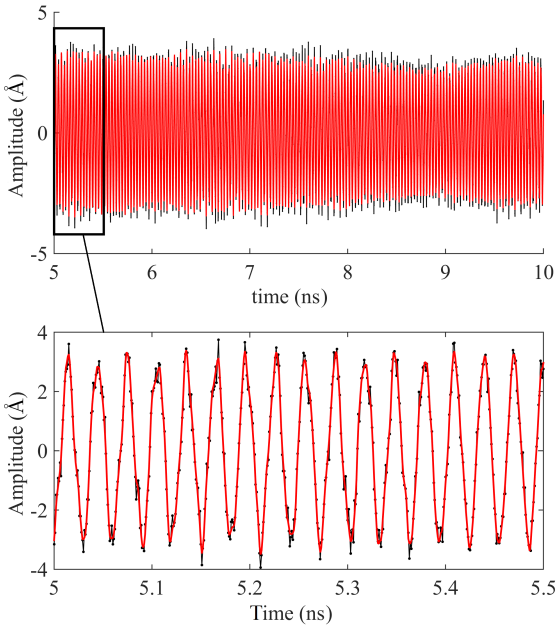


Figure 9: Time response of the center of the graphene membrane excited with an initial velocity of 0.5 Å/ps, obtained from MD (black line) and POD by considering first mode only (red line) in a time range of 5 to 10 ns.

bending stiffness suggested by statistical mechanics of elastic membranes [46].

Next, using the obtained POMs and Equations (7a)–(16), the reduced order model is built and the convergence of the model is studied to verify the accuracy of employing single transverse degree of freedom for expressing the nonlinear effects at large amplitude. Figure 11 illustrates the backbone curves of the periodic solutions of the nonlinear set of equations in (16), for free vibrations. The graphs in Figure 11-A are obtained considering different number of transverse and in-plane degrees of freedom (n and m in Equations (7a) and (7b)). As it can be observed, the response of the system converges with considering one transverse and three in-plane degrees of freedom. This convergence analysis verifies that the large amplitude vibrations and the induced geometrical stiffness in the motion of the graphene membrane can be mimicked by including a single transverse mode, only. In fact, Figure 11 shows that at large amplitudes of vibrations (e.g. at time range of 0-10 ns in MD simulations), even if the higher modes are included in the reduced order model, they do not have much contribution in the additional geometrical stiffness at large amplitudes. As a consequence, Equation (16) can be simplified to Equation (17) while still capturing the effects of geometrical stiffness at large amplitudes, accurately. We shall remind that

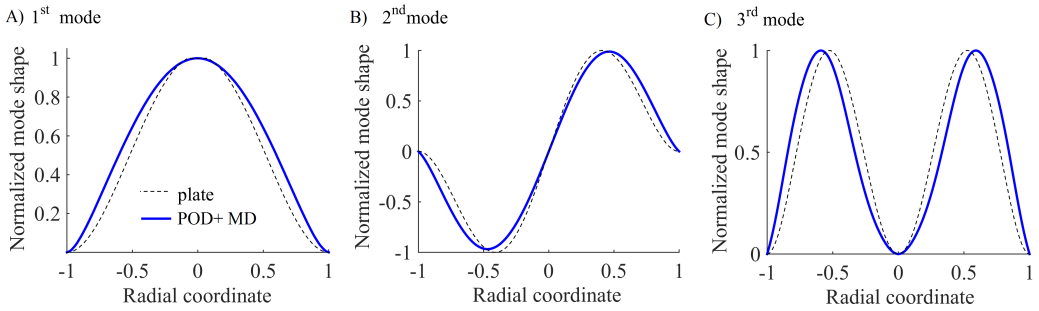


Figure 10: The first 3 POMs of the graphene membrane excited with an initial velocity of 0.5 Å/ps, obtained from time response of the MD in a time range of 5 to 10 ns, in comparison to a classical plate mode shapes.

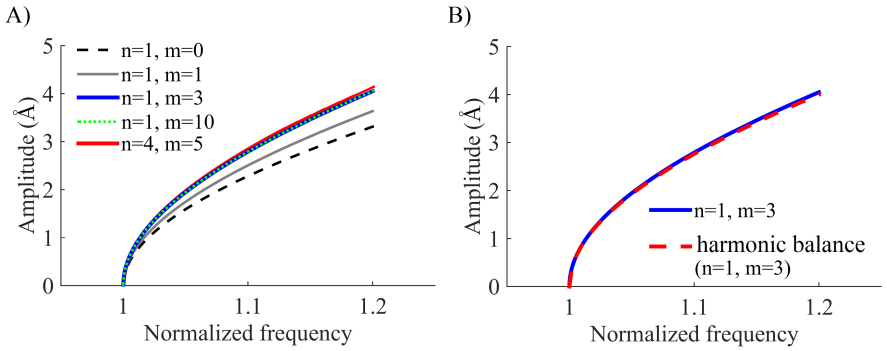


Figure 11: Amplitude of vibrations as a function of the its frequency when $E = 800\,\text{GPa}$, $N_0 = 0.35\,\text{N/m}$, and D= A) Convergence of the solution by using 1 transverse and 3 in-plane modes in the reduced order model, and B) good agreement of the results of harmonic balance method with the reduced order model.

in this method the influence of thermal vibration on the natural frequency (i.e. linear stiffness, or ω_0^2 in Equation(17)) and the mode shape (which appears in the relation of k_3) are included. Moreover, For comparison the backbone curve obtained by using harmonic balance approximation is also shown in Figure 11-B. Figure 11-B shows that the harmonic balance approximation is adequately accurate for obtaining the backbone of the system.

Eventually, the equivalent Young's modulus is identified by fitting the backbone curve obtained directly from MD simulations and from the reduced order model as expressed in Equation (18). Figure 12 shows the backbone curves from both models using E as the fitting parameter. The MD data is obtained by exciting the membrane with different initial velocities, ranging from 0.5 Å/ps to 1 Å/ps. The graphs in this figure are obtained for two different temperature of 5 and 300 K. The extracted equivalent Young's moduli which fits the numerical backbone curve to the data from MD at 5 and 300 K are $E = 925\,\text{GPa}$ and $E = 771\,\text{GPa}$, respectively. For comparison two backbone curves of an equivalent system with $E = 600\,\text{GPa}$ and $E = 1000\,\text{GPa}$ are also shown in Figure 12.

It can be observed from Figure 12-B that the data obtained from MD simulations at 300 K are more scattered. This is because the time evolution of the kinetic energy in 300 K occurs faster as compared to 5 K and hence, at 300 K in the time range of 5-10 ns the motion is not quite steady as compared to 5 K. Therefore, we chose two time ranges of 5 to 7.5 ns, and 5 to 10 for this temperature in order to increase the accuracy of fitting.

The obtained Young's modulus as a function of temperature is illustrated in Figure 13. As

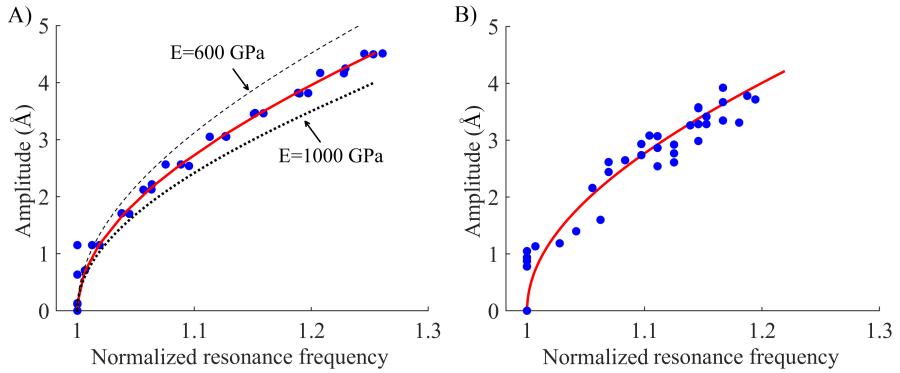


Figure 12: Maximum amplitude of vibrations as a function of the frequency of the peak amplitude at temperature of A) 5 K, where $\omega_0 = 31.794\,\text{GHz}$ and $E = 925\,\text{GPa}$ and B) 300 K, where $\omega_0 = 28.794\,\text{GHz}$ and $E = 771\,\text{GPa}$, obtained from harmonic balance (red line) and MD (blue dots).

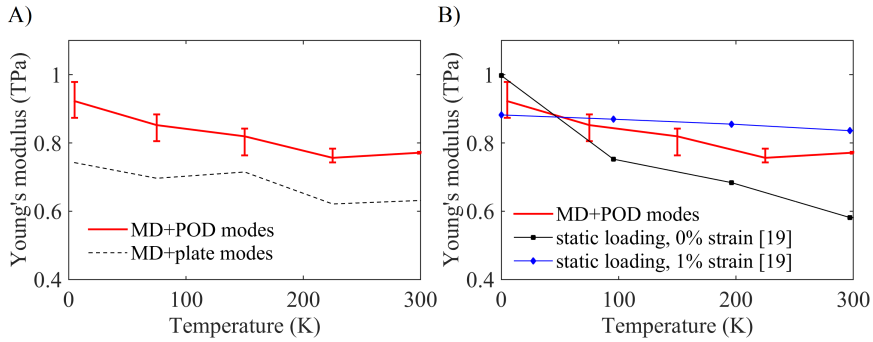


Figure 13: The obtained Young's modulus as a function of the temperature A) by using different set of mode shapes in the Lagrangian approach, and B) via dynamic and static approaches.

it can be observed, the Young's modulus is monotonically decreasing with temperature. For comparison the Young's modulus has been extracted by same methodology though with assuming the vibrational mode-shapes of a classical plate as the set of basis functions in building the reduced order model. The difference between the extracted Young's moduli in Figure 13-A shows the importance of using the POD algorithm for calculating the proper mode-shapes of the graphene membrane. Moreover, for comparison, the tangent elastic moduli of graphene at strains of 0% and 1% obtained by Ref. [19] are given in Figure 13-B. The latter obtains the elastic modulus in MD simulations via static loading. As it can be observed, our obtained dynamic modulus is closer to the tangent elastic modulus at 1% strain where the thermally induced ripples are suppressed due to the relatively large static deformation. It shall be noticed that our obtained dynamic Young's modulus at room temperature ($E = 771\,\mathrm{GPa}$) is smaller than the elastic modulus in static loading as suggested by Ref. [19] ($E = 840\,\mathrm{GPa}$) and Ref. [24] ($E = 890\,\mathrm{GPa}$). This difference may originate from different elastic behavior of graphene in dynamic and static loading, but also due to the interplay between the dynamic ripples and the stiffness of the lattice of the graphene membrane, which cannot be captured if the ripples are suppressed in the static loading.

In addition, the simulations have been repeated for different radii of the membrane (i.e. R=10-18 nm) at T=150 K, and the obtained Young's moduli are given in Table 1. As it can be observed the Young's modulus of graphene slightly reduces with the size of the membrane. These results are in agreement with observations of Ref. [19]. In fact, increasing the radius of the membrane at smaller scales, similar to the temperature, will enhance the thermal fluctuations and therefore, reduces the Young's modulus.

Table 1: The obtained Young's modulus for different radii of the graphene membrane at T=150 K.

Radius (nm)	Young's modulus (GPa)
10	822.1 (±32.2)
12	717.0 (±22.3)
14	790.0 (±15.8)
16	782.5 (±33.0)
18	779.4 (±16.7)

4. Conclusion

In this paper, we proposed a reduction method based on atomistic simulations for characterization of graphene membranes. In this model, we employed the POMs obtained from a POD of the data extracted from molecular dynamics simulations. Therefore, the obtained reduced order

equations of motion can accurately model the dynamics of the nano-membrane with much less degrees of freedom and hence, they are suitable for investigating the nonlinear dynamics.

By using the obtained reduced order model, we proposed an identification algorithm which makes use of the nonlinear response of the membrane at large amplitude vibrations for estimating its Young's modulus. This approach can obtain the dynamic Young's modulus while capturing the effects of dynamic ripples due to Brownian motion on the natural frequencies and mode shapes, accurately. Moreover, using this method, it was shown that the dynamic elastic modulus of the membrane reduces monotonically with temperature and size of the membrane, and it is slightly lower than the static elastic modulus provided by Ref. [24] and Ref. [19]. Our methodology has the potential to serve as the next generation of characterization techniques for other nano-structures in finite temperature.

Acknowledgements

Authors acknowledge the financial support through TU Delft, 3mE cohesion grant NITRO.

References

[1] Robin J Dolleman, Dejan Davidovikj, Santiago J Cartamil-Bueno, Herre SJ van der Zant, and Peter G Steeneken. Graphene squeeze-film pressure sensors. *Nano letters*, 16(1):568–571, 2015. ISSN 1530-6984.

[2] Juan Atalaya, Jari M Kinaret, and Andreas Isacsson. Nanomechanical mass measurement using nonlinear response of a graphene membrane. *EPL (Europhysics Letters)*, 91(4):48001, 2010. ISSN 0295-5075.

[3] F Schedin, AK Geim, SV Morozov, EW Hill, P Blake, MI Katsnelson, and KS Novoselov. Detection of individual gas molecules adsorbed on graphene. *Nature materials*, 6(9):652–655, 2007. ISSN 1476-1122.

[4] Frank Schwierz. Graphene transistors. *Nature nanotechnology*, 5(7):487–496, 2010. ISSN 1748-3387.

[5] Changyao Chen, Sunwoo Lee, Vikram V Deshpande, Gwan-Hyoung Lee, Michael Lekas, Kenneth Shepard, and James Hone. Graphene mechanical oscillators with tunable frequency. *Nature nanotechnology*, 8(12):923–927, 2013. ISSN 1748-3387. doi: 10.1038/nnano.2013.232.

[6] Konstantin S Novoselov, VI Fal, L Colombo, PR Gellert, MG Schwab, and K Kim. A roadmap for graphene. *Nature*, 490(7419):192–200, 2012. ISSN 0028-0836.

[7] Jin-Wu Jiang, Jian-Sheng Wang, and Baowen Li. Young's modulus of graphene: a molecular dynamics study. *Physical Review B*, 80(11):113405, 2009.

[8] H Zhao, K Min, and NR Aluru. Size and chirality dependent elastic properties of graphene nanoribbons under uniaxial tension. *Nano letters*, 9(8):3012–3015, 2009. ISSN 1530-6984.

[9] Shikai Deng and Vikas Berry. Wrinkled, rippled and crumpled graphene: an overview of formation mechanism, electronic properties, and applications. *Materials Today*, 19(4):197–212, 2016. ISSN 1369-7021.

[10] Cesare Davini, Antonino Favata, and Roberto Paroni. The gaussian stiffness of graphene deduced from a continuum model based on molecular dynamics potentials. *Journal of the Mechanics and Physics of Solids*, 104:96–114, 2017. ISSN 0022-5096.

[11] Banafsheh Sajadi, Farbod Alijani, Dejan Davidovikj, Johannes Goosen, Peter G Steeneken, and Fred van Keulen. Experimental characterization of graphene by electrostatic resonance frequency tuning. *Journal of Applied Physics*, 122(23):234302, 2017. ISSN 0021-8979.

[12] Dejan Davidovikj, Farbod Alijani, Santiago J Cartamil-Bueno, Herre SJ van der Zant, Marco Amabili, and Peter G Steeneken. Nonlinear dynamic characterization of two-dimensional materials. *Nature Communications*, 8.1, 2017. doi: 10.1038/s41467-017-01351-4.

[13] Changgu Lee, Xiaoding Wei, Jeffrey W Kysar, and James Hone. Measurement of the elastic properties and intrinsic strength of monolayer graphene. *Science*, 321(5887):385–388, 2008. ISSN 0036-8075.

[14] Andres Castellanos-Gomez, Michele Buscema, Rianda Molenaar, Vibhor Singh, Laurens Janssen, Herre SJ van der Zant, and Gary A Steele. Deterministic transfer of two-dimensional materials by all-dry viscoelastic stamping. *2D Materials*, 1(1):011002, 2014. ISSN 2053-1583. doi: 10.1088/2053-1583/1/1/011002.

[15] Deji Akinwande, Christopher J Brennan, J Scott Bunch, Philip Egberts, Jonathan R Felts, Huajian Gao, Rui Huang, Joon-Seok Kim, Teng Li, and Yao Li. A review on mechanics and mechanical properties of 2d materials—graphene and beyond. *Extreme Mechanics Letters*, 13:42–77, 2017. ISSN 2352-4316.

[16] Traian Dumitrică and Richard D James. Objective molecular dynamics. *Journal of the Mechanics and Physics of Solids*, 55(10):2206–2236, 2007. ISSN 0022-5096.

[17] Wenzhong Bao, Feng Miao, Zhen Chen, Hang Zhang, Wanyoung Jang, Chris Dames, and Chun Ning Lau. Controlled ripple texturing of suspended graphene and ultrathin graphite membranes. *Nature nanotechnology*, 4(9):562–566, 2009. ISSN 1748-3387.

[18] Shuo Chen and DC Chrzan. Monte carlo simulation of temperature-dependent elastic properties of graphene. *Physical Review B*, 84(19):195409, 2011.

[19] Wei Gao and Rui Huang. Thermomechanics of monolayer graphene: Rippling, thermal expansion and elasticity. *Journal of the Mechanics and Physics of Solids*, 66:42–58, 2014. ISSN 0022-5096.

[20] Fatemeh Ahmadpoor, Peng Wang, Rui Huang, and Pradeep Sharma. Thermal fluctuations and effective bending stiffness of elastic thin sheets and graphene: A nonlinear analysis. *Journal of the Mechanics and Physics of Solids*, 107:294–319, 2017. ISSN 0022-5096.

[21] Banafsheh Sajadi, Simon van Hemert, Behrouz Arash, Pierpaolo Belardinelli, Peter G. Steeneken, and Farbod Alijani. Size- and temperature-dependent bending rigidity of graphene using modal analysis. *Carbon*, 139:334–341, 2018. ISSN 0008-6223. doi: https://doi.org/10.1016/j.carbon.2018.06.066. URL `http://www.sciencedirect.com/science/article/pii/S0008622318306328`.

[22] Dengke Chen and Yashashree Kulkarni. Entropic interaction between fluctuating twin boundaries. *Journal of the Mechanics and Physics of Solids*, 84:59–71, 2015. ISSN 0022-5096.

[23] Ryan JT Nicholl, Hiram J Conley, Nickolay V Lavrik, Ivan Vlassiouk, Yevgeniy S Puzyrev, Vijayashree Parsi Sreenivas, Sokrates T Pantelides, and Kirill I Bolotin. The effect of intrinsic crumpling on the mechanics of free-standing graphene. *Nature communications*, 6, 2015.

[24] JH Los, A Fasolino, and MI Katsnelson. Mechanics of thermally fluctuating membranes. *npj 2D Materials and Applications*, 1(1):9, 2017. ISSN 2397-7132.

[25] Banafsheh Sajadi, Farbod Alijani, Hans Goosen, and Fred van Keulen. Effect of pressure on nonlinear dynamics and instability of electrically actuated circular micro-plates. *Nonlinear Dynamics*, 91(4):2157–2170, 2018. ISSN 0924-090X. doi: 10.1007/s11071-017-4007-y.

[26] Gregory W Vogl and Ali H Nayfeh. A reduced-order model for electrically actuated clamped circular plates. In *ASME 2003 International Design Engineering Technical Conferences and Computers and Information in Engineering Conference*, pages 1867–1874. American Society of Mechanical Engineers, 2003. doi: 10.1088/0960-1317/15/4/002.

[27] Banafsheh Sajadi, Hans Goosen, and Fred van Keulen. Electrostatic instability of micro-plates subjected to differential pressure: A semi-analytical approach. *International Journal of Mechanical Sciences*, 138:210–218, 2018. ISSN 0020-7403. doi: https://doi.org/10.1016/j.ijmecsci.2018.02.007.

[28] Steve Plimpton, Paul Crozier, and Aidan Thompson. Lammps-large-scale atomic/molecular massively parallel simulator. *Sandia National Laboratories*, 18:43–43, 2007.

[29] J Tersoff. Empirical interatomic potential for carbon, with applications to amorphous carbon. *Physical Review Letters*, 61(25):2879, 1988.

[30] R Klessig and E Polak. Efficient implementations of the polak–ribière conjugate gradient algorithm. *SIAM Journal on Control*, 10(3):524–549, 1972. ISSN 0036-1402.

[31] Denis J Evans and Brad Lee Holian. The nose–hoover thermostat. *The Journal of chemical physics*, 83(8):4069–4074, 1985. ISSN 0021-9606.

[32] DA Bistrian and IM Navon. Comparison of optimized dynamic mode decomposition vs pod for the shallow water equations model reduction with large-time-step observations. *International Journal for Numerical Methods in Fluids*, pages 1–25, 2014.

[33] V Lenaerts, Gaëtan Kerschen, and Jean-Claude Golinval. Proper orthogonal decomposition for model updating of non-linear mechanical systems. *Mechanical Systems and Signal Processing*, 15(1):31–43, 2001. ISSN 0888-3270.

[34] Peter J Schmid, Larry Li, Matthew P Juniper, and O Pust. Applications of the dynamic mode decomposition. *Theoretical and Computational Fluid Dynamics*, 25(1-4):249–259, 2011. ISSN 0935-4964.

[35] Vejapong Juttijudata, John L Lumley, and Dietmar Rempfer. Proper orthogonal decomposition in squire's coordinate system for dynamical models of channel turbulence. *Journal of Fluid Mechanics*, 534:195–225, 2005. ISSN 1469-7645.

[36] Willem Cazemier. *Proper orthogonal decomposition and low dimensional models for turbulent flows*. [University Library Groningen][Host], 1997. ISBN 9036706823.

[37] Vladimir Buljak and Giulio Maier. Proper orthogonal decomposition and radial basis functions in material characterization based on instrumented indentation. *Engineering Structures*, 33(2):492–501, 2011. ISSN 0141-0296.

[38] BF Feeny. Interpreting proper orthogonal modes in vibrations. In *Proceedings of DET*, volume 97.

[39] Vincent Lenaerts, Gaëtan Kerschen, and Jean-Claude Golinval. Ecl benchmark: application of the proper orthogonal decomposition. *Mechanical Systems and Signal Processing*, 17(1): 237–242, 2003. ISSN 0888-3270.

[40] M Amabili, A Sarkar, and MP Paıdoussis. Reduced-order models for nonlinear vibrations of cylindrical shells via the proper orthogonal decomposition method. *Journal of Fluids and Structures*, 18(2):227–250, 2003. ISSN 0889-9746.

[41] Marco Amabili. *Nonlinear vibrations and stability of shells and plates*. Cambridge University Press, 2008. ISBN 1139469029. doi: 10.1017/CBO9780511619694. URL `http://dx.doi.org/10.1017/CBO9780511619694`.

[42] Stephen Timoshenko, Sergius Woinowsky-Krieger, and S Woinowsky. *Theory of plates and shells*, volume 2. McGraw-hill New York, 1959. URL `https://books.google.nl/books?id=rTQFAAAAMAAJ`.

[43] Ali H Nayfeh and Dean T Mook. *Nonlinear oscillations*. John Wiley & Sons, 2008. ISBN 3527617590. doi: 10.1002/9783527617586.

[44] Harry Dankowicz and Frank Schilder. *Recipes for continuation*, volume 11. SIAM, 2013. ISBN 1611972566.

[45] MJ Brennan, I Kovacic, A Carrella, and TP Waters. On the jump-up and jump-down frequencies of the duffing oscillator. *Journal of Sound and Vibration*, 318(4):1250–1261, 2008. ISSN 0022-460X.

[46] Rafael Roldán, Annalisa Fasolino, Kostyantyn V Zakharchenko, and Mikhail I Katsnelson. Suppression of anharmonicities in crystalline membranes by external strain. *Physical Review B*, 83(17):174104, 2011.